Distinguishing fluid and solid breast masses with fundamental and harmonic amplitude- and coherence-based ultrasound beamforming

Arunima Sharma[*], Alycen Wiacek[*], Eniola Oluyemi[†], Kelly Myers[†], Emily Ambinder[†], Muyinatu A. Lediju Bell[*‡§]

[*]Department of Electrical and Computer Engineering, Johns Hopkins University, Baltimore, MD

[†]Department of Radiology and Radiological Science, Johns Hopkins Medicine, Baltimore, MD

[‡]Department of Biomedical Engineering, Johns Hopkins University, Baltimore, MD

[‡]Department of Computer Science, Johns Hopkins University, Baltimore, MD

2022 IEEE International Ultrasonics Symposium (IUS) | 978-1-6654-6657-8/22/$31.00 ©2022 IEEE | DOI: 10.1109/IUS54386.2022.9958237

***Abstract*—Harmonic imaging has demonstrated potential to improve B-mode and short-lag spatial coherence (SLSC) image quality by reducing acoustic clutter. In addition, our group previously demonstrated that robust SLSC (R-SLSC) distinguishes solid from fluid masses in breast ultrasound. However, a combined harmonic R-SLSC imaging approach has not been previously explored. This work is the first to investigate the ability of both harmonic B-mode and harmonic R-SLSC images to distinguish solid from fluid-filled breast masses in comparison to their fundamental imaging counterparts. Raw ultrasound data from 18 breast masses were acquired and beamformed to obtain matched fundamental and harmonic B-mode and R-SLSC images. Clutter reduction with harmonic imaging resulted in up to 4.2 dB contrast improvement in harmonic B-mode images compared to fundamental B-mode images, yet led to increased spatial coherence within the hypoechoic masses. Therefore, the contrast of fluid masses in harmonic R-SLSC images was 7.02-12.5 dB worse than that of fundamental R-SLSC images. The generalized contrast-to-noise ratio was implemented as an objective discriminator of fluid and solid masses with 100% and 94% accuracy achieved with fundamental and harmonic R-SLSC imaging, respectively. These results suggest that although harmonic imaging reduces clutter, fundamental R-SLSC is better suited to distinguish solid from fluid breast mass contents.**

I. Introduction

Ultrasound offers the advantages of safe, portable, cost-efficient, and real-time imaging, thus it is widely utilized in diagnostic applications. In particular, breast ultrasound imaging is often implemented in conjunction with mammography to detect and diagnose breast masses [1], [2]. However, the use of breast ultrasound as a screening tool is limited due to high false positive rates of 10% in tissues with low visually estimated mammographic breast density (i.e., $<$25% glandular) and 14.4% in tissues with high visually estimated mammographic breast density (i.e., $>$80% glandular) [2]. One reason for these high false positive rates is the presence of acoustic clutter [3], [4] which complicates the ability of radiologists to provide accurate diagnoses based on ultrasound images alone.

When the higher harmonics generated by non-linear wave propagation through tissue are leveraged to create images, harmonic ultrasound imaging suppresses side and grating lobes and minimizes the effects of reverberant echoes. Therefore, harmonic ultrasound imaging is widely used to decrease acoustic clutter and improve breast mass detection [5], [6]. However, harmonic imaging is known to be less effective at achieving these goals in patients with predominantly glandular breasts [7].

Short-lag spatial coherence (SLSC) imaging [8] successfully reduces acoustic clutter in cases where harmonic imaging fails, demonstrating improved visualization in applications spanning thyroid imaging [8], lesion detection [9], liver imaging [10], fetal imaging [11], [12], and breast imaging [13]. However, this technique suffers from providing a grainy appearance at the higher lag values that offer better spatial resolution. Robust SLSC (R-SLSC) [14] was developed to improve the appearance of SLSC images created with higher lag values by applying robust principal component analysis to vectorized SLSC images created with multiple lags, then applying a linearly decaying weighted summation of the filtered images. As a result, R-SLSC images successfully included the high-frequency information available at higher lags while offering improved contrast, contrast-to-noise ratios (CNRs), and tissue signal-to-noise ratios (SNRs) when compared to traditional SLSC images.

Previous work from our group demonstrated that R-SLSC imaging improves the diagnostic certainty of breast ultrasound imaging by distinguishing fluid-filled masses from solid masses [13], [15]–[17]. A reader study conducted with five board-certified breast radiologists further validated that the combination of R-SLSC with traditional ultrasound B-mode imaging improved the sensitivity of detecting fluid-filled masses from 57% with only B-mode images to 86% when including R-SLSC images alongside B-mode images, thereby reducing the percentage of unnecessary biopsy from 43.3% to 13.3% [16], [17].

With both harmonic imaging and coherence-based imaging introduced as individual and combined possibilities to improve fundamental B-mode imaging, at least four ultrasound imaging modes are possible to diagnose and analyze breast lesions. However, the benefits or limitations of each possible mode to distinguish fluid from solid masses are unclear. In addition, multiple imaging modes are anticipated to increase radiologist reading times.

Therefore, the objective of this work is to qualitatively and quantitatively compare fundamental and harmonic B-mode with fundamental and harmonic R-SLSC images of *in vivo* solid and fluid-filled breast masses. Our two quantitative metrics are contrast, which was previously introduced as a discriminator of fluid vs. solid mass contents [13], and the generalized contrast-to-noise ratio (gCNR), which was recently introduced as a more reliable and objective metric of lesion detectability [18], [19]. We additionally investigate the feasibility of implementing the more objective gCNR metric to eventually minimize the time that would otherwise be required for radiologists to read the multiple imaging modes investigated in this study.

II. Methods

Ultrasound breast data were acquired from patients enrolled in our ongoing study after receiving informed consent and approval from Johns Hopkins Medicine Institutional Review Board (Protocol No. IRB00127110). Eighteen hypoechoic masses from 13 patients scheduled for ultrasound-guided aspiration or core-needle biopsy were included in this study. Each patient was scanned using an Alpinion ECUBE12R research ultrasound scanner (Alpinion, Seoul, Korea). This scanner was connected to an Alpinion L8-17 probe with center frequency of 12.5 MHz and sampling frequency of 40 MHz. A pulse-inversion sequence was transmitted to form matched fundamental and harmonic images. Fundamental channel data were formed with echoes received from the normal pulse, and harmonic channel data were formed with summed echoes from the normal and inverted pulse. The fundamental and harmonic channel data were delayed and processed offline to form matched fundamental and harmonic B-mode and R-SLSC images.

To implement R-SLSC imaging [14], the first step of SLSC imaging was implemented as described in previous work [8], [20] with a correlation kernel size equal to one wavelength to create a coherence function for each lateral and axial position in the image. These coherence functions were utilized to create lag m images, representing the coherence value at each lag as an image for all axial and lateral locations. These lag images were vectorized and stacked to form a matrix, D. Robust principal component analysis was then performed to solve for A in the expression

$$D = A + E \tag{1}$$

where A is the underlying low-rank matrix that estimates the ground-truth and E is the error matrix. Each filtered lag image in the resulting matrix A was then weighted by $1 - \frac{(m-1)}{M}$, where m is the lag value of the filtered lag image, ranging from 1 to M. The values within the weighted matrix A were summed over the lag dimension, and the vectorization was reversed to form the R-SLSC image with $M = 20$.

The contrast of breast masses relative to background tissue was measured and compared across matched fundamental and harmonic B-mode and R-SLSC images:

$$Contrast = 20\ log\left(\frac{S_{mass}}{S_{tissue}}\right) \tag{2}$$

where S_{mass} and S_{tissue} are the mean signal within a region of interest (ROI) inside the mass and background tissue, respectively.

The gCNR of breast masses relative to surrounding tissue was measured as follows [18]:

$$gCNR = 1 - \sum_{k=0}^{N-1} min\{h_{mass}(x_k), h_{tissue}(x_k)\} \tag{3}$$

where N bins centered at $\{x_1, x_2 ... x_n\}$ were defined, h_{mass} and h_{tissue} are the associated histograms of the mass and the surrounding breast tissue, respectively, and k is the index of the bin. A linear support vector machine (SVM) model was applied to the gCNR measurements to determine a threshold that objectively distinguishes solid from fluid masses in fundamental and harmonic R-SLSC images. The accuracy of this threshold was then determined.

III. Results and Discussion

Fig. 1 shows example fundamental and harmonic B-mode and R-SLSC images of three *in vivo* hypoechoic breast masses. As expected, harmonic B-mode images generally have reduced clutter compared to fundamental B-mode images. Also as expected, in both fundamental and harmonic R-SLSC images, the fluid mass is discernible from the background and the detectability of solid masses is low. However, the masses in the R-SLSC fundamental images are more detectable when compared to their harmonic counterparts.

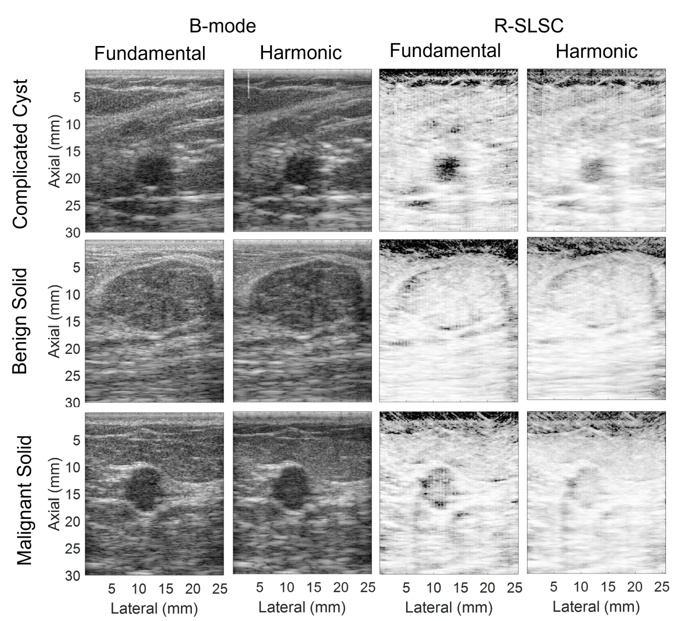

Fig. 1. Fundamental and harmonic B-mode and R-SLSC images of a fluid-filled mass, a benign solid mass, and a malignant solid mass. All images are displayed with 60 dB dynamic range.

Fig. 2(a) shows the contrast measured in B-mode and R-SLSC images of the 18 masses included in this study, in blue and red, respectively, displayed as overlapping bar graphs. Solid and dashed bars denote fundamental and harmonic values, respectively. The purple bars represent the regions where the values of B-mode and R-SLSC images overlap. Thus, more prominent red regions indicate larger values of R-SLSC compared to B-mode images, which is particularly true of the fluid masses. In these fluid mass cases, the purple bars (dashed and solid) show values in B-mode images and red bars (dashed and solid) show values in R-SLSC images.

Conversely, more prominent blue regions in Fig. 2(a) indicate larger values of B-mode compared to R-SLSC images, which is particularly true of the solid masses. In these solid mass cases, purple bars (dashed and solid) represent R-SLSC values while blue bars (dashed and solid) represent values in B-mode images. In addition, the difference between the mean contrast of fluid-filled and the mean contrast of solid masses is 27.46 dB in fundamental R-SLSC images and 18.48 dB in harmonic R-SLSC images. The difference in contrast between fluid-filled and solid masses in coherence-based images is responsible for previously reported findings that R-SLSC imaging distinguishes solid from fluid-filled masses [13], [21], which is now demonstrated to be true for both fundamental and harmonic cases. However, the 7.02-12.5 dB improved contrast of the fluid-filled masses in fundamental R-SLSC compared to harmonic R-SLSC images indicates that fundamental R-SLSC imaging is better suited to visualize fluid masses, which agrees with qualitative observations of Fig. 1.

Fig. 2(b) shows corresponding gCNR values reported in a similar format to the contrast measurements in Fig. 2(a). The mean gCNR of the fundamental and harmonic B-mode images across the fluid-filled masses are 0.68 and 0.74, respectively. Similarly, the mean gCNR of the fundamental and harmonic B-mode images across the solid masses are 0.66 and 0.68, respectively. These similar gCNR values (i.e., 0.66-0.74) indicate similar mass detectability when employing amplitude-based beamforming. On the other hand, the mean gCNR of the fundamental and harmonic R-SLSC images across the fluid-filled masses are 0.98 and 0.99, respectively, and the mean gCNR of the fundamental and harmonic R-SLSC images across the solid masses are 0.40 and 0.42, respectively. The 0.98-0.99 mean gCNR values of fluid-filled masses and the lower (i.e., 0.40-0.42) gCNR values of solid masses in R-SLSC images support the introduction of gCNR as a potential objective metric for solid vs. fluid mass distinction with R-SLSC imaging.

Fig. 3 shows the gCNR measured in fundamental and harmonic R-SLSC images of fluid-filled and solid masses, with the dashed line indicating the threshold obtained by fitting a linear SVM model. Dataset imbalance due to different numbers of solid and fluid-filled masses was addressed by dividing the gCNR of the solid and fluid-filled masses by the percentage of the number of solid and fluid-filled masses, respectively. The optimal threshold was determined to be 0.73, resulting in high accuracy (i.e., 100% for fundamental and 94.4% for harmonic) when identifying whether the mass is solid or fluid-filled, which further supports the introduction of gCNR as a potential objective metric.

Fig. 4 shows example coherence functions averaged over regions of interest within the mass and tissue regions of one fluid-filled and one solid mass. These coherence functions provide a rationale for the differences observed in solid and fluid-filled masses in fundamental and harmonic R-SLSC imaging. In addition, lower coherence is observed within the fluid mass when compared to the surrounding tissue in both the fundamental and harmonic images. However, the coherence function obtained with harmonic imaging has larger values

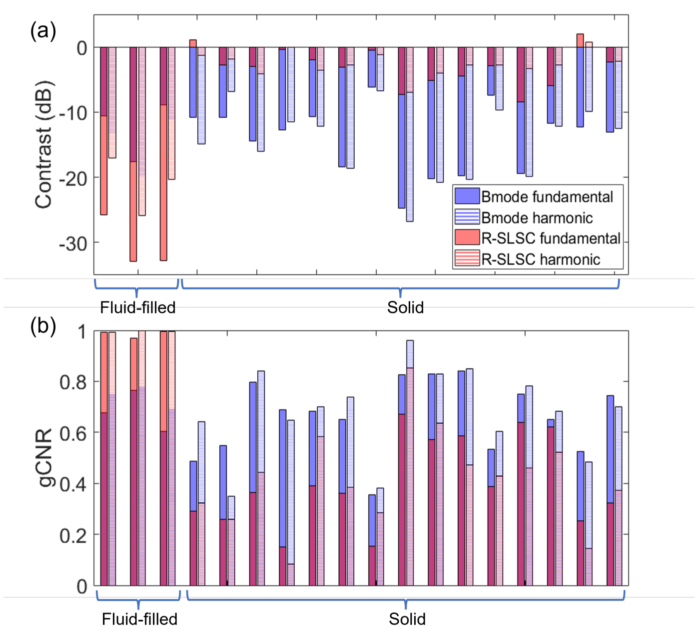

Fig. 2. Contrast and generalized contrast-to-noise ratio (gCNR) of the 18 masses included in our study, plotted as overlapping bar graphs, with the purple color detailing regions of overlap.

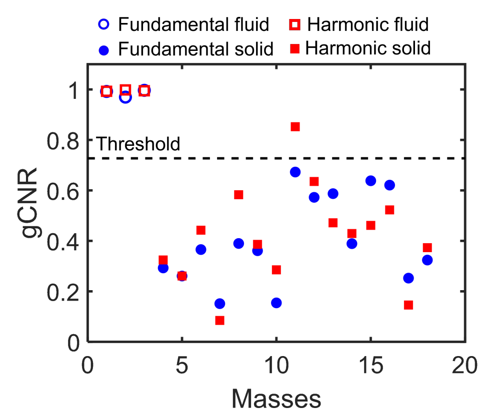

Fig. 3. The gCNR of fundamental and harmonic R-SLSC images with threshold separating fluid from solid masses determined by support vector machine.

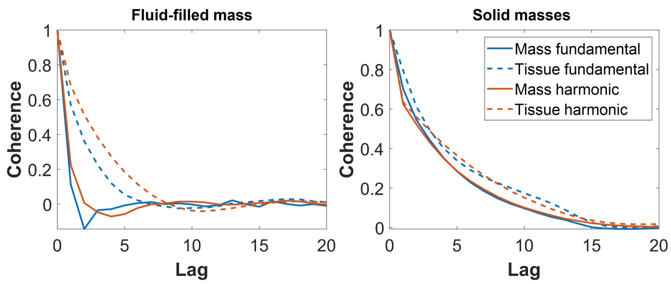

Fig. 4. Mean coherence functions within regions of interest from fluid-filled and solid masses and surrounding tissue.

than that obtained with fundamental imaging (likely due to the clutter reduction achieved with harmonic imaging). As a result, the coherence within the fluid-filled mass is closer to that of the surrounding tissue, which decreases the contrast of the harmonic R-SLSC image. This observation supports the greater accuracy achieved with fundamental R-SLSC imaging when using gCNR as an objective discriminator between solid and fluid mass content (Fig. 3) and the better visibility of fluid-filled masses in fundamental R-SLSC compared to harmonic R-SLSC images (Figs. 1 and 2(a)).

IV. Conclusion

This work is the first to demonstrate the application of harmonic coherence-based imaging to determine the solid or fluid content of hypoechoic breast masses. Matched B-mode and R-SLSC fundamental and harmonic images of 18 breast masses were compared qualitatively and quantitatively (i.e., using contrast and gCNR). The harmonic B-mode images demonstrated improved contrast compared to the corresponding fundamental images in a majority of breast masses (i.e., 14 out of 18 masses). However, the fundamental R-SLSC images showed improved contrast compared to the harmonic R-SLSC images in the majority of breast masses (i.e., 13 out of 18 total). This improved contrast is particularly true of the three fluid masses. The reduced acoustic clutter achieved with harmonic imaging seems to increase the spatial coherence of fluid-filled masses, complicating the discernment of the mass from the tissue in harmonic R-SLSC imaging when compared to fundamental R-SLSC imaging. Therefore, our results suggest that the potential of fundamental R-SLSC imaging is greater than that of harmonic R-SLSC imaging when employed to differentiate fluid-filled from solid masses, which is also supported by the accuracy of the newly introduced objective gCNR discriminator method.

Acknowledgment

This work is supported by NIH R01EB032960.

References

[1] W. A. Berg, J. D. Blume, J. B. Cormack, E. B. Mendelson, D. Lehrer, M. Böhm-Vélez, E. D. Pisano, R. A. Jong, W. P. Evans, M. J. Morton *et al.*, "Combined screening with ultrasound and mammography vs mammography alone in women at elevated risk of breast cancer," *JAMA*, vol. 299, no. 18, pp. 2151–2163, 2008.

[2] W. A. Berg, A. I. Bandos, E. B. Mendelson, D. Lehrer, R. A. Jong, and E. D. Pisano, "Ultrasound as the primary screening test for breast cancer: analysis from ACRIN 6666," *JNCI: Journal of the National Cancer Institute*, vol. 108, no. 4, 2016.

[3] S. Huber, M. Wagner, M. Medl, and H. Czembirek, "Real-time spatial compound imaging in breast ultrasound," *Ultrasound in Medicine & Biology*, vol. 28, no. 2, pp. 155–163, 2002.

[4] M. A. Lediju, M. J. Pihl, J. J. Dahl, and G. E. Trahey, "Quantitative assessment of the magnitude, impact and spatial extent of ultrasonic clutter," *Ultrasonic Imaging*, vol. 30, no. 3, pp. 151–168, 2008.

[5] T. F, G. N, E. V, and P. L., "Clinical use of ultrasound tissue harmonic imaging," *Ultrasound in Medicine & Biology*, vol. 25, no. 6, 1999.

[6] Z. Laura and O. T. Robert, "Harmonic ultrasound: a review," *Veterinary Radiology & Ultrasound*, vol. 43, no. 6, 2002.

[7] S. T. Kazimierz, P. M. Anna, W. Maciej, A. Dominique, S. Malgorzata, and J. Wieslaw, "Tissue harmonic imaging: utility in breast sonography," *Journal of Ultrasound in Medicine*, vol. 22, no. 5, 2003.

[8] M. A. Lediju, G. E. Trahey, B. C. Byram, and J. J. Dahl, "Short-lag spatial coherence of backscattered echoes: Imaging characteristics," *IEEE Transactions on Ultrasonics, Ferroelectrics, and Frequency Control*, vol. 58, no. 7, pp. 1377–1388, 2011.

[9] J. J. Dahl, D. Hyun, M. Lediju, and G. E. Trahey, "Lesion detectability in diagnostic ultrasound with short-lag spatial coherence imaging," *Ultrasonic Imaging*, vol. 33, no. 2, pp. 119–133, 2011.

[10] M. Jakovljevic, G. E. Trahey, R. C. Nelson, and J. J. Dahl, "In vivo application of short-lag spatial coherence imaging in human liver," *Ultrasound in Medicine & Biology*, vol. 39, no. 3, pp. 534–542, 2013.

[11] W. Long, D. Hyun, K. R. Choudhury, D. Bradway, P. McNally, B. Boyd, S. Ellestad, and G. E. Trahey, "Clinical utility of fetal short-lag spatial coherence imaging," *Ultrasound in Medicine & Biology*, 2018.

[12] V. Kakkad, J. Dahl, S. Ellestad, and G. Trahey, "In vivo application of short-lag spatial coherence and harmonic spatial coherence imaging in fetal ultrasound," *Ultrasonic Imaging*, vol. 37, no. 2, pp. 101–116, 2015.

[13] A. Wiacek, O. M. H. Rindal, E. Falomo, K. Myers, K. Fabrega-Foster, S. Harvey, and M. A. L. Bell, "Robust short-lag spatial coherence imaging of breast ultrasound data: Initial clinical results," *IEEE Transactions on Ultrasonics, Ferroelectrics, and Frequency Control*, vol. 66, no. 3, pp. 527–540, 2019.

[14] A. A. Nair, T. D. Tran, and M. A. L. Bell, "Robust short-lag spatial coherence imaging," *IEEE Transactions on Ultrasonics, Ferroelectrics, and Frequency Control*, 2018.

[15] A. Wiacek, E. Falomo, K. Myers, O. M. H. Rindal, K. Fabrega-Foster, S. Harvey, and M. A. L. Bell, "Clinical feasibility of coherence-based beamforming to distinguish solid from fluid hypoechoic breast masses," in *2018 IEEE International Ultrasonics Symposium (IUS)*. IEEE, 2018, pp. 1–4.

[16] A. Wiacek, E. Oluyemi, K. Myers, L. Mullen, and M. A. L. Bell, "Coherence-based beamforming improves the diagnostic certainty of breast ultrasound exams," in *2020 IEEE International Ultrasonics Symposium (IUS)*. IEEE, 2020, pp. 1–4.

[17] A. Wiacek, E. Falomo, K. Myers, O. M. H. Rindal, K. Fabrega-Foster, S. Harvey, and M. A. L. Bell, "Clinical feasibility of coherence-based beamforming to distinguish solid from fluid hypoechoic breast masses," in *2018 IEEE International Ultrasonics Symposium (IUS)*. IEEE, 2018, pp. 1–4.

[18] A. Rodriguez-Molares, O. M. H. Rindal, J. D'hooge, S.-E. Måsøy, A. Austeng, M. A. L. Bell, and H. Torp, "The generalized contrast-to-noise ratio: a formal definition for lesion detectability," *IEEE Transactions on Ultrasonics, Ferroelectrics, and Frequency Control*, vol. 67, no. 4, pp. 745–759, 2019.

[19] M. R. Gubbi, E. A. Gonzalez, and M. A. L. Bell, "Theoretical framework to predict generalized contrast-to-noise ratios of photoacoustic images with applications to computer vision," *IEEE Transactions on Ultrasonics, Ferroelectrics, and Frequency Control*, vol. 69, no. 6, pp. 2098–2114, 2022.

[20] M. A. L. Bell, J. J. Dahl, and G. E. Trahey, "Resolution and brightness characteristics of short-lag spatial coherence (SLSC) images," *IEEE Transactions on Ultrasonics, Ferroelectrics, and Frequency Control*, vol. 62, no. 7, pp. 1265–1276, 2015.

[21] A. Wiacek, E. Oluyemi, K. Myers, L. Mullen, and M. A. L. Bell, "Coherence-based beamforming increases the diagnostic certainty of distinguishing fluid from solid masses in breast ultrasound exams," *Ultrasound in Medicine & Biology*, vol. 46, no. 6, pp. 1380–1394, 2020.